

All-Fiber Source and Sorter for Multimode Correlated Photons

Kfir Sulimany¹ and Yaron Bromberg^{1*}

¹Racah Institute of Physics, The Hebrew University of Jerusalem, Jerusalem 91904, Israel

*Corresponding authors: yaron.bromberg@mail.huji.ac.il

Abstract

Photons occupying multiple spatial modes hold a great promise for implementing high-dimensional quantum communication. We use spontaneous four-wave mixing to generate multimode photon pairs in a few mode fiber. We show the photons are correlated in the fiber mode basis using an all-fiber mode sorter. Our demonstration offers an essential building block for realizing high-dimensional quantum protocols based on standard, commercially available fibers, in an all-fiber configuration.

1 Introduction

High-dimensional quantum bits hold great potential for quantum communication owing to their robustness to a realistic noisy environment [1, 2, 3]. Implementations based on encoding information in the transverse spatial modes of photons are especially promising due to the large Hilbert space they span [4, 5]. In recent years, such implementations were successfully demonstrated in free-space [6, 7]. Meanwhile, efforts for multimode fiber-based technologies are expected to achieve high-dimensional quantum communication without line of sight, based on existing multimode fiber components and infrastructures [8, 9, 10, 11, 12, 13, 14].

The leading approach for generating entangled photons in transverse spatial modes is through spontaneous parametric down conversion in bulk crystals [15]. However, it is extremely challenging to couple transverse entangled photons to fibers since it requires a precise mapping between the free space transverse modes and the fiber guided modes. Indeed, most demonstrations of distributing spatially entangled photons with fibers are limited to coupling of only two guided modes [8, 9, 10, 11]. Recently, distribution of a photon which is entangled in six spatial modes over a 2 meter-long fiber [12], and in three spatial modes over a 1 km-long fiber were demonstrated [13]. However, these methods require accurate calibrations, limiting implementations in real-life scenarios.

An alternative for coupling free-space entangled photons to a fiber, is to generate the photons inside the fiber by using spontaneous four-wave mixing (SFWM). Over the past two decades, generation of photon pairs by SFWM was studied using multiple types of single mode optical fibers [16], including photonic crystal fibers [17, 18, 19, 20], dispersion shifted fibers [21, 22, 23], and

birefringent fibers [24, 25]. SFWM in multimode fibers was recently utilized for generating photons occupying a high dimensional transverse mode [26, 27, 28]. Generating photon pairs in a superposition of multiple fiber modes requires precise analysis of the phase matching conditions that will allow multiple SFWM processes in the same spectral channel [29, 30, 31, 32]. These theoretical works predict that the photon pair sources can be tunable for a wide range wavelengths, from the ultraviolet to the infra red and the telecommunication range. Experimentally, such phase matching conditions were recently studied for parametric amplification of weak signals [33], but not in the spontaneous regime. Hence correlations between pairs of photons generated in multiple fiber modes were not measured to date.

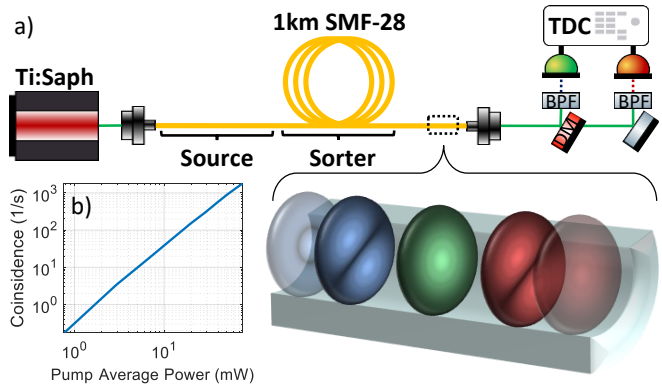
In this work, we propose and demonstrate a fiber source of photon pairs which occupy multiple fiber modes. Our measurements prove that the photons are correlated in the guided mode basis, by mapping the modes the photons occupy to their arrival times at the end of a 1 km-long fiber. The 1 km-long fiber acts as an all-fiber in-line mode sorter, in contrast to bulk free-space mode sorters that are typically used for measuring correlations between transverse modes [34, 15, 35, 36]. Our in-line mode sorting configuration allows us to measure the two-dimensional (2D) histogram of the arrival times of the photons, which reveals that the photons occupy three guided modes of the fiber. By analyzing the histogram we achieve the two-photon modal decomposition and verify the spatial correlations of photon pairs generated in the multimode fiber.

2 Results

2.1 Multimode Correlated Photons Source

Our source is based on coupling Ti:Sapphire mode-locked pulses (pulse duration 140fs , wavelength $\lambda_{pump} = 695\text{nm}$) into a few mode fiber as shown in Figure 1. In SFWM, two pump photons are spontaneously annihilated, and two photons called signal and idler are generated in two spectral channels ($\lambda_s = 542\text{nm}$, $\lambda_i = 970\text{nm}$). Each spectral channel is composed of many different spatial modes. The photons occupy the guided modes of the fiber, which can be approximated by the linearly polarized (LP) modes of a weakly guiding optical fiber. The state of the photons is determined by the phase matching conditions and can be written as: $|\Psi\rangle = \alpha|LP_{02}\rangle_s|LP_{01}\rangle_i + \beta|LP_{11}\rangle_s|LP_{11}\rangle_i$ where subscripts s (i) mark the mode of the signal (idler) photon and the coefficients α, β are determined by the nonlinear overlap integral (see Supplementary Equation 3). The term $|LP_{01}\rangle_s|LP_{02}\rangle_i$ is not present in the quantum state as the mode LP_{02} is not guided in our fiber for the wavelength of the idler photon. Extension of this scheme to higher dimensions and other spectral bands is presented in the Supplementary Note 1.

The photon pairs are generated mostly in the first few tens of centimeters of the fiber, after which the peak power of the pump pulse is too weak for SFWM due to its temporal spreading, for more information see Supplementary Note 2. To quantify the efficiency of the pair generation we use a 20cm section of SMF-28 to measure the coincidence detection rate as a function of the average pump power, exhibiting a quadratic scaling as expected for a four-wave mixing process (Fig. 1b). The coincidence to accidental ratio we obtain for a pump power of 10mW is 850 (see Supplementary Note 3 for more details). In principle, to improve the coincidence rate we could use higher pump powers. Increasing the pump power, however, will also increase parasitic Raman scattering. In our system Raman scattering hardly adds noise since it is temporally separated from the generated photon pairs. However, the pump power is limited since the photon counts due to Raman scattering exceed the maximal count rate of our detectors ($\approx 5\text{MHz}$). This limitation can be circumvented by using superconducting nanowire detectors with an order of magnitude higher maximal count rates ($\approx 50\text{MHz}$), or by using in-line fiber Bragg gratings to filter the pump light before the sorter, so that the pump will not generate Raman scattering along the 1 km -long fiber.



Supplementary Figure 1: **An all-fiber multimode source and mode sorter for photon pairs correlated in the fiber modes.** a) Ultrashort pulses of 140fs ($\lambda_{pump} = 695\text{nm}$) are coupled into a 1 km -long fiber. Pump photons are spontaneously annihilated and pairs of signal and idler photons are generated at two different spectral channels ($\lambda_s = 542\text{nm}$, $\lambda_i = 970\text{nm}$). At these wavelengths, the fiber (SMF-28) supports a few modes, where the modal distribution of the photon pairs is determined by the phase matching condition of the fiber. After the first few tens of centimeters, the temporal spread of the pump pulse prevents SFWM. In the next 1-km long section of the fiber, the different modes are separated due to modal dispersion (inset). Higher spatial modes arrive after lower spatial modes, and shorter wavelengths arrive after longer wavelengths. At the output of the fiber the signal and idler photons are spectrally separated by a dichroic mirror (DM), filtered by a band-pass filter (BPF) and their arrival times are registered using two single photon detectors and a time-to-digital converter (TDC). An electronic delay of 70ns is introduced to the idler detector to compensate for chromatic delay between the signal and idler photons. b) The experimentally measured coincidence rate as a function of the pump average power for a 20nm long fiber exhibiting quadratic scaling.

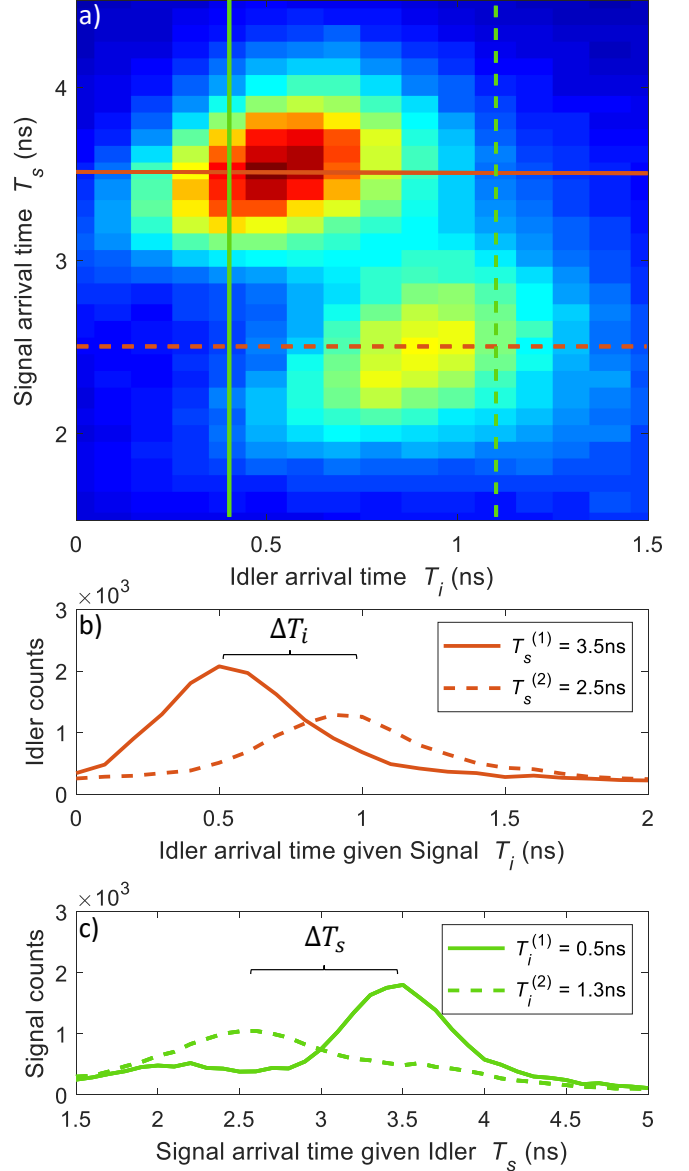
2.2 Multimode Photons Sorter

Next, we use a 1 km -long section of the same fiber, which serves as a photon pairs source and as a mode sorter of the fiber's guided modes. Due to modal Group Delay Dispersion (GDD), the arrival times of the photons at the end of the fiber depend on their modal distribution and their spectral channel, as depicted in Figure 1. We can therefore map the arrival times of the photons to their modal decomposition, up to modal degeneracy in symmetric fiber cores. Although this sorting scheme is quite common in classical optics [37], it was only recently demonstrated at the single photon level for weak coherent pulses [38]. Here we use the same principle for entangled photons. In our set-up, the temporal resolu-

tion is limited by the jitter of the avalanche photo diodes which is $400ps$. Since the GDD of our fiber is in the scale of $1ns/km$, a 1 km-long fiber is sufficient to temporally separate the modes.

2.3 Two Photon Modal Distribution Measurement

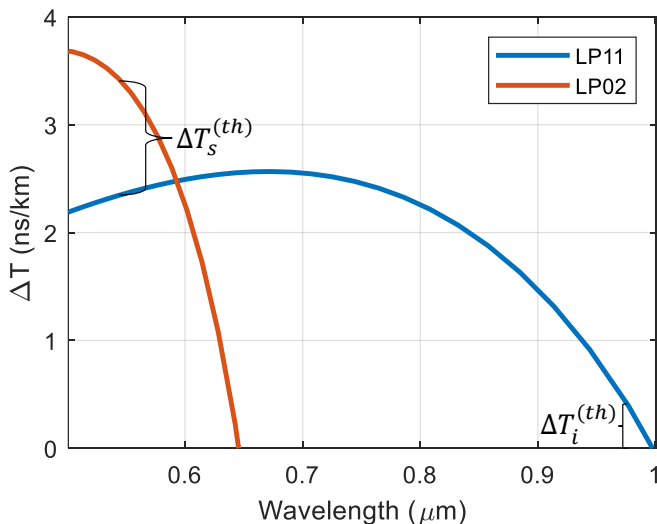
To investigate the modal distribution of the two-photon state, we use the mode-to-time mapping and study the temporal two-photon probability $P(T_s, T_i)$ that describes the probability to detect a signal photon at time T_s and an idler photon at time T_i . To this end, we plot the two-dimensional histogram of the arrival times after compensating for chromatic dispersion (Figure 2(a)). Two correlation peaks are observed, corresponding to the delay between either $|LP_{02}\rangle_s$ and $|LP_{01}\rangle_i$ or between $|LP_{11}\rangle_s$ and $|LP_{11}\rangle_i$. Clearly, the two-photon probability is not-separable, indicating that photons are correlated in the modal basis. To quantify the correlation of the two photons we post select two arrival times for the signal ($T_s^{(1)}, T_s^{(2)}$) and two arrival times for the idler ($T_i^{(1)}, T_i^{(2)}$). The post-selected arrival times are chosen to maximize the Pearson correlation coefficient: $PCC = \frac{\sum_{k=1}^2 \sum_{l=1}^2 P(T_s^{(k)}, T_i^{(l)}) (T_s^{(k)} - \mu_{T_s})(T_i^{(l)} - \mu_{T_i})}{\sigma_{T_s} \sigma_{T_i}}$ where μ_{T_s}, μ_{T_i} are the mean arrival times of the signal and idler photons and $\sigma_{T_s}, \sigma_{T_i}$ are their standard deviations. We obtain $PCC = 0.51 \pm 0.012$, which indicates a strong correlation. The main source of correlation degradation in our system is the $400ps$ jitter of the detectors, which causes a circular smearing of the histogram peaks. Another source of decorrelation is the uncertainty in the creation times of the pairs, which results in a diagonal spread of about $\approx 200ps$ that hardly effects the PCC between the chosen arrival times. In principle, inter modal coupling can also add decorrelation, however the PCC is sensitive only to mode mixing that occurs in the first few tens of centimeters of the fiber, because the arrival times of photons which experience mode coupling after a longer distance will be different from the post selected times $(T_s^{(1)}, T_s^{(2)}), (T_i^{(1)}, T_i^{(2)})$. Thus PCC degradation due to inter modal mode mixing, which is typically on the order of $20db/km$ [39], is negligible.



Supplementary Figure 2: **Temporal two-photon probability.** (a) Histogram of the arrival times T_s, T_i of the signal and idler photons. The arrival times are measured relative to an electronic trigger from the pump laser which serves as a global clock, and after adding an electronic delay of $70ns$ to the idler detector to compensate for the chromatic delay between the signal and idler photons. The two off-diagonal peaks indicate that the two-photon state is not separable. We therefore conclude that the photons are correlated in the modal basis. The two peaks correspond to occupation of modes $|LP_{02}\rangle_s |LP_{01}\rangle_i$ and $|LP_{11}\rangle_s |LP_{11}\rangle_i$, as verified by numerical computation of the fiber's modal group delays. (b),(c) Cross sections of the two-dimensional histogram along the lines marked in (a), emphasizing the modal correlations. For example, post selecting events with an idler's arrival time of $T_i^{(1)} = 0.4ns$ (green solid curve) shows localization of the signal photon at $T_s^{(1)} = 3.5ns$. In (b) the post selection is on the signal photon, while in (c) it is on the idler photon. The measured delay between the two peaks is $\Delta T_s = 1ns$ for the signal photons and $\Delta T_i = 0.5ns$ for the idler photons.

2.4 Modal Group Delay Simulation

To show that the measured delays between the signal and idler photons match the expected delays for an SMF-28 fiber, we numerically calculated its modal group delays. We solve the scalar wave equation for an SMF-28 fiber, with a $4.2\mu\text{m}$ core radius, core-cladding index difference of $\Delta = 0.33\%$, and a step-index profile with a typical dip shape. The modal delay of LP_{11}, LP_{02} modes, relative to the fundamental mode is presented in Figure 3. We chose the fundamental mode as a reference to cancel the chromatic dispersion. At the signal’s wavelength the delay between the LP_{02} and LP_{11} is $\Delta T_s = 1\text{ns}$. At the idler’s wavelength the delay of LP_{01} and LP_{11} is $\Delta T_i = 0.5\text{ns}$. These delays are in agreement with the temporal correlations found experimentally, supporting mode-to-time mapping scheme.



Supplementary Figure 3: **Numerical computation of the modal delays of the LP_{11} (blue curve) and the LP_{02} (red curve) modes.** The delays are presented relative to the fundamental mode LP_{01} , to compensate for chromatic delay. For the signal photon at $\lambda_s = 542\text{nm}$, the delay between the LP_{02} and LP_{11} modes is $\Delta T_s^{(th)} = 1\text{ns/km}$, in agreement with the experimentally measured delays presented in Figure 2(c). For the idler photon at $\lambda_i = 970\text{nm}$, the delay between the LP_{11} and LP_{01} modes is $\Delta T_i^{(th)} = 0.5\text{ns/km}$, in agreement with measured delays reported in Figure 2(b).

3 Discussion

In conclusion, we have demonstrated generation and sorting of correlated photon pairs occupying high order modes of a commercially available fiber. The all-fiber configuration opens the door for implementing high-dimensional photonic quantum bits in fiber-based applications. For example, the mode-to-time mapping can potentially solve the challenge of scaling the number of

required detectors with the number of fiber modes, an outstanding challenge in conventional mode sorters. Towards this end, it is necessary to improve the temporal resolution of the system, for example by using superconducting nanowire single photon detectors with jitter times as low as a few picoseconds, and faster electronics. It will allow sorting more transverse modes and using shorter fibers for the temporal mode sorter, which in turn will decrease the background noise caused by fluorescence and parasitic nonlinear processes in the fiber.

In order to manipulate the photons coherently and apply projective measurement in two mutually unbiased bases one can use multi-plane light converters (MPLC) [40, 34, 41, 35]. We note that by combining the all-fiber temporal sorter with an all-fiber wavefront modulator that we recently developed [42], it would be possible to demonstrate an all-fiber sorter in mutually unbiased basis, opening the door for all fiber quantum communication protocols with high dimensional quantum bits.

Addressing these challenges will allow exploring applications of the all-fiber source and sorter. For example, using an in-line multimode fiber beam splitter one could split the photon pairs and route each photon to a different remote user. Such configuration is relevant for device independent quantum key distribution, where an untrusted user (Charlie) distributes entangled photon pairs to Alice and Bob, who generate a secure key based on Bell measurements [43]. A more immediate application of the all-fiber source is quantum communication protocols that rely on sending both photons to the same target. Examples include quantum dense coding [44, 45], high capacity quantum key distribution [46, 47] and direct quantum communication [48].

4 Methods

4.1 Experimental Setup

An optical fiber (SMF-28) is pumped by a Ti:Sapphire laser (Coherent Chameleon Ultra II, 680-1060nm, 140fs duration, 80MHz repetition rate). Before coupling to the fiber, the laser was filtered using a bandpass filter (Thorlabs FB700-40). The signal and idler photons were separated using a dichroic mirror (DM) with an edge at 925 nm (Semrock FF925-Di01). In each arm the pump beam was blocked using spectral filters. In the signal arm we employed a short pass filter (Semrock BSP01-633R), and a bandpass filter (Semrock FF01-540). In the Idler arm we employed a long pass filter (Semrock BLP01-808R) and a bandpass filter (Semrock LL01-976). The signal and idler photons were coupled into two optical fibers (SMF-28) and detected using avalanche photodetectors (Excelitas SPCM-AQ4C), with a quantum efficiency of 50% for the signal photons and 15% for the idler photons. The arrival times of the photons were registered

using a time-to-digital converter (Swabian Time Tagger 20).

5 Acknowledgments

The authors kindly thank Hagai Eisenberg and Avi Pe'er for many fruitful discussions and suggestions. This re-

search was supported by the *United States-Israel Binational Science Foundation (BSF)* (Grant No. 2017694). KS and YB acknowledge the support of the Israeli Council for Higher Education, the Israel National Quantum Initiative (INQI) and the Zuckerman STEM Leadership Program.

6 Supplementary Information

6.1 Note 1: Scheme for higher-dimensional state generation at telecom and visible wavelengths

To generate high-dimensional states in a superposition of multiple fiber modes, it is required to find the phase matching condition that will allow multiple spontaneous four-wave mixing processes in the same spectral channel. Here we show a concrete example of such phase-matching condition based on a commercially available graded index (GRIN) fiber (OM4) spliced to a commercial Ytterbium mode-locked fiber laser. In addition to the possibility to generate high-dimensional quantum states, this scheme also allows generation of photons in the c-band.

We start by presenting the phase matching condition that allows high-dimensional entanglement in OM4 fibers. In multimode fibers, one can find multiple modal configurations that satisfy the phase matching condition required for four-wave mixing. There are a few benefits in using GRIN fibers. The guided-modes in a GRIN fiber can propagate with nearly identical group velocities and therefore nonlinear coupling among short pulses is achieved over much longer distances than in step index fibers. More importantly for generating high-dimensional quantum bits, the parabolic refractive index profile of GRIN fibers yields degenerate group modes with equally spaced propagation constants β_n and a degeneracy that scales linearly with the group number g_n . It is therefore possible to obtain multiple combinations of guided-modes that satisfy the phase matching condition for the same signal and idler frequencies ω_s, ω_i . Explicitly, the dependence of the phase matched signal and idler frequencies on the group number mismatch defined by $G = -2g_{\text{pump}} + g_{\text{idler}} + g_{\text{signal}}$ is given by [49]:

$$\omega_{s,i} = \omega_p \pm \sqrt{\frac{\sqrt{2}\Delta G}{R\beta_p^{(2)}(\omega_p)}} \quad (1)$$

Where the $+$ ($-$) sign corresponds to the signal (idler) frequency, ω_p is the pump frequency, $\beta_p^{(2)}(\omega_p)$ is the group-velocity dispersion parameter of the pump mode, and R, Δ are the core radius and the maximal refractive index difference between the core and the clad, respectively. The dimension of the signal and idler photons therefore increases with the group number mismatch G . For example, for $G = 2$ there are four different modal combinations that yield the same phase matched frequencies, resulting in four-dimensional quantum states at ω_s and ω_i .

To confirm the above phase matching analysis, we numerically solve the multimode nonlinear Schrödinger equation (MM-NLSE) using the numerical solver developed in [50]. The MM-NLSE is given by:

$$\frac{\partial A_k}{\partial z} = i \sum_n \frac{\beta_n^{(k)}}{n!} (i \frac{\partial}{\partial t})^n A_k + i \frac{n_2 \omega_p}{c} \sum_{lmn} S_{klmn} A_l A_m A_n^* \quad (2)$$

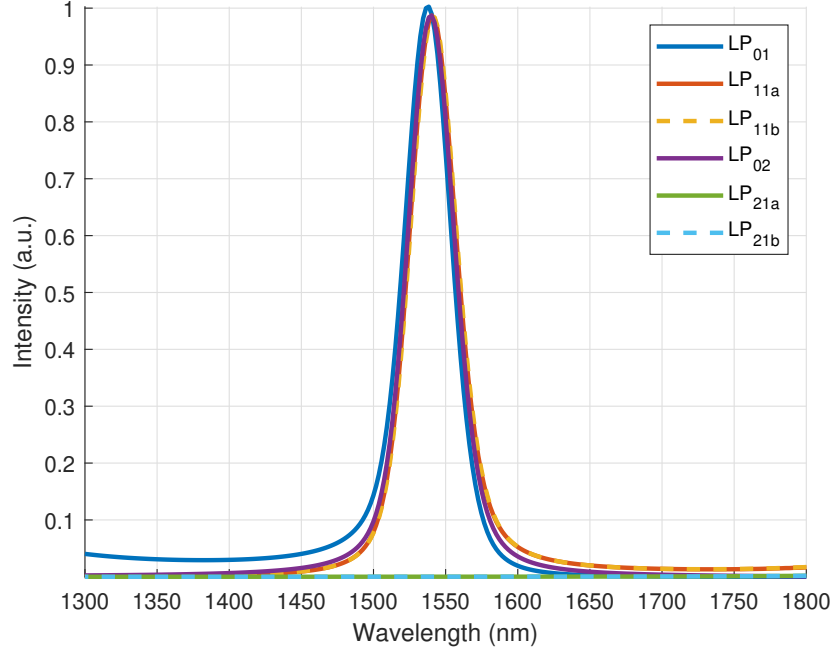
where $A_k(z, t)$ is the slowly varying amplitude of mode k , z is the propagation axis along the fiber and $\beta_n^{(k)} = \partial^n \beta^{(k)} / \partial \omega^n$. The nonlinear coupling coefficients S_{klmn} are given by the overlap of the transverse profiles of the guided-modes $F_k(x, y)$:

$$S_{klmn} = \frac{\int dx dy F_k^*(x, y) F_n^*(x, y) F_m(x, y) F_l(x, y)}{\sqrt{\int dx dy |F_k(x, y)|^2 \int dx dy |F_l(x, y)|^2 \int dx dy |F_m(x, y)|^2 \int dx dy |F_n(x, y)|^2}} \quad (3)$$

To obtain the phase matched frequencies, we propagate a strong pump field at the fundamental mode of a GRIN fiber at $\lambda_p = 1040\text{nm}$, together with a weak signal seed occupying all the guided-modes of the fiber and all wavelengths lower than λ_p . To simulate a concrete scheme, we use 140fs pulses with an energy of 0.1nJ per pulse, corresponding to commercially available Ytterbium mode-locked fiber lasers. Supplementary Figure 4 presents the spectrum at the output of a 10cm long fiber, exhibiting idler photons centered at $\lambda = 1540\text{nm}$ that occupy four fiber modes.

In Supplementary Table 1 we summarize the spontaneous four-wave mixing processes that are stimulated by the seed parameters given above, showing that four-dimensional quantum states can be generated in the c-band, by pumping a GRIN fiber with a commercially available femtosecond fibre laser.

The spectral band of the generated photons depends on the pump wavelength. It is possible to generate spontaneous intermodal four wave mixing up to the telecom wavelengths, thanks to the fact that the phase matching conditions are nearly unaffected by the pump wavelength. For example, in the above table we present a process where the idler is generated in the telecom c-band spectrum. However, because the four-wave mixing process conserves energy, the second photon is generated in 785nm . Such configuration is especially relevant when one wishes to send one photon in free-space and the other photon in a fiber.



Supplementary Figure 4: Power spectrum of intermodal four-wave mixing at the output of a 10cm graded index fiber pumped by $140fs$ pulses at $\lambda_p = 1040nm$, obtained by numerical integration of the multimode nonlinear Schrödinger equation (MM-NLSE). To find the phase matching wavelengths, all the guided-modes of the fiber at wavelengths lower than λ_p were excited.

Signal mode	Idler mode	λ_{Signal} (nm)	λ_{Idler} (nm)	G
LP_{01}	LP_{02}	785	1540	2
LP_{02}	LP_{01}	785	1540	2
LP_{11a}	LP_{11a}	785	1540	2
LP_{11b}	LP_{11b}	785	1540	2

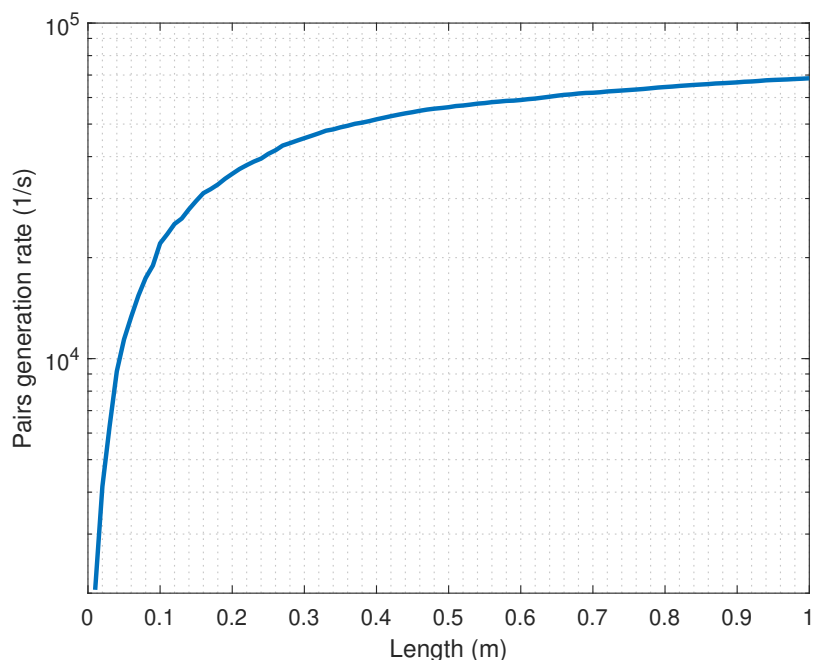
Supplementary Table 1: Phase-matching of intermodal four-wave mixing in a GRIN fiber (OM4). The pump is assumed to be in the LP_{01} mode at $\lambda_p = 1040nm$. At $\lambda_s = 785nm$ and $\lambda_i = 1540nm$ we get four types of intermodal processes, enabling the generation of a four-dimensional quantum state.

6.2 Note 2: Numerical calculation of the pair generation rate

To analyze the pair generation rate as a function of the fiber length, we numerically integrate the MM-NLSE as described in the previous section, now for the fibre and pump parameters used in our experiment. We propagate a strong pump pulse occupying the fundamental mode, along with weak white noise occupying all guided-modes that simulates seeding by vacuum fluctuations. For the pump field we assume $140fs$, $0.1nJ$ pulses centered at $\lambda_p = 695nm$, with a repetition rate of $80MHz$, corresponding to the pulses used in our experiment. For the vacuum fluctuations we assume zero mean fields with nonzero variance which corresponds to an energy of $\hbar\omega$ per spectral channel [51]. The obtained pair rate at the output of the fiber as a function of the fiber length is presented in Supplementary Figure 5, showing that most of the photons are generated in the first tens of centimeters of the fiber. We attribute most of the reduction in the pair rate to the pump dispersion, as the dispersion length for the pump pulses, defined by $L_D = T_0^2/\beta_2$ where $T_0 = 140fs$ is the pulse duration and $\beta_2 = 44000fs^2$ is the group velocity dispersion parameter, is approximately 45cm.

We further note that an upper bound on the fiber segment length over which the photons are generated, can be estimated from the temporal two-photon probability presented in Figure 2 of the main text. Since the temporal signal-idler separation scales linearly with the distance they propagate in the fiber, generation at different positions along the fiber exhibits smearing of the two-photon probability peaks along its diagonal. Figure 2 exhibits a diagonal spreading of $\approx 200ps$. Since the measured signal-idler separation after 1km is $70ns$, the $200ps$ spreading sets an

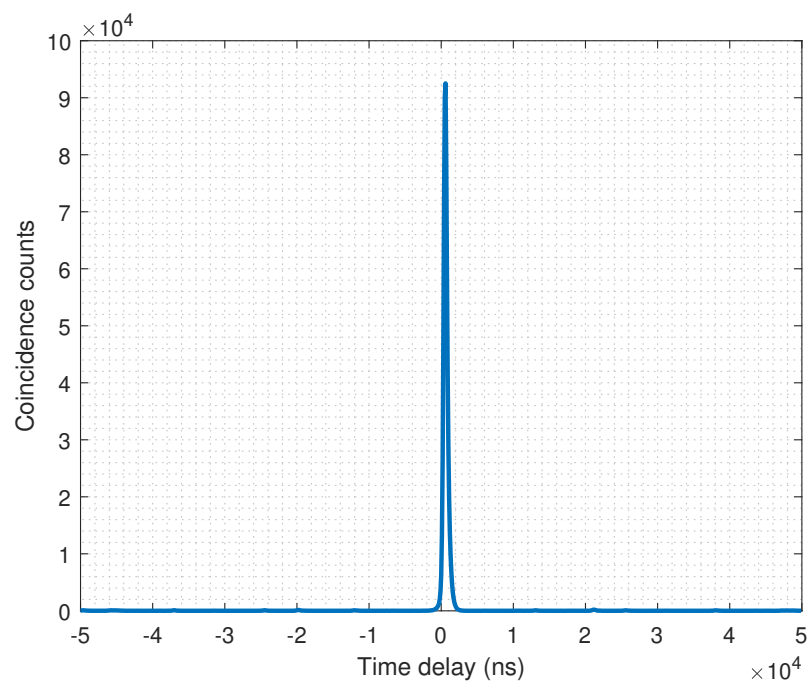
upper of a few meters on the segment length over which the pairs are generated. In practice, since other noise sources may contribute to the diagonal spreading of the two-photon probability, the actual segment length is most likely shorter than this upper bound.



Supplementary Figure 5: Pair generation rate obtained by numerical integration of the multimode nonlinear Schrödinger equation. Here we propagate $0.1nJ$, 140fs long pump pulses at $\lambda_p = 695nm$, together with white noise fields at $\lambda_{vacuum} < 695nm$ corresponding to vacuum fluctuations, which have a zero mean and a nonzero variance corresponding to an energy of $\hbar\omega$ per spectral channel.

6.3 Note 3: Coincidence to accidental ratio measurement

To quantify the coincidence to accidental ratio (CAR) we measured the coincidence histogram below for a pump average power of $P = 10mW$, using 20cm long section of a SMF-28 (Supplementary Figure 6). The CAR is found by the ratio of the correlation peak to the highest correlation measured at a delay of an integer number of pump periods, $CAR = 850$.



Supplementary Figure 6: Coincidence histogram ranging a few times the separation between consecutive pump pulses, yielding a coincidence to accidental ratio of $CAR = 850$ for a pump average power of $P = 10mW$.

References

- [1] Nicolas J Cerf et al. “Security of quantum key distribution using d-level systems”. In: *Physical review letters* 88.12 (2002), p. 127902.
- [2] Manuel Erhard, Mario Krenn, and Anton Zeilinger. “Advances in high-dimensional quantum entanglement”. In: *Nature Reviews Physics* (2020), pp. 1–17.
- [3] Daniele Cozzolino et al. “High-dimensional quantum communication: benefits, progress, and future challenges”. In: *Advanced Quantum Technologies* 2.12 (2019), p. 1900038.
- [4] Gabriel Molina-Terriza, Juan P Torres, and Lluís Torner. “Twisted photons”. In: *Nature physics* 3.5 (2007), pp. 305–310.
- [5] Manuel Erhard et al. “Twisted photons: new quantum perspectives in high dimensions”. In: *Light: Science & Applications* 7.3 (2018), pp. 17146–17146.
- [6] Mario Krenn et al. “Twisted photon entanglement through turbulent air across Vienna”. In: *Proceedings of the National Academy of Sciences* 112.46 (2015), pp. 14197–14201.
- [7] Alicia Sit et al. “High-dimensional intracity quantum cryptography with structured photons”. In: *Optica* 4.9 (2017), pp. 1006–1010.
- [8] W Löffler et al. “Fiber transport of spatially entangled photons”. In: *Physical review letters* 106.24 (2011), p. 240505.
- [9] Yoonshik Kang et al. “Measurement of the entanglement between photonic spatial modes in optical fibers”. In: *Physical review letters* 109.2 (2012), p. 020502.
- [10] Daniele Cozzolino et al. “Air-core fiber distribution of hybrid vector vortex-polarization entangled states”. In: *Advanced Photonics* 1.4 (2019), p. 046005.
- [11] A Alarcón et al. “Few-mode fibre technology fine-tunes losses of quantum communication systems”. In: *arXiv preprint arXiv:2103.05018* (2021).
- [12] Natalia Herrera Valencia et al. “Unscrambling entanglement through a complex medium”. In: *Nature Physics* (2020), pp. 1–5.
- [13] Huan Cao et al. “Distribution of high-dimensional orbital angular momentum entanglement over a 1 km few-mode fiber”. In: *Optica* 7.3 (2020), pp. 232–237.
- [14] Yiyu Zhou et al. “High-fidelity spatial mode transmission through a 1-km-long multimode fiber via vectorial time reversal”. In: *Nature Communications* 12.1 (2021), pp. 1–7.
- [15] Alois Mair et al. “Entanglement of the orbital angular momentum states of photons”. In: *Nature* 412.6844 (2001), pp. 313–316.
- [16] Kyungdeuk Park et al. “Telecom C-band photon-pair generation using standard SMF-28 fiber”. In: *Optics Communications* (2020), p. 126692.
- [17] Jay E Sharping et al. “Quantum-correlated twin photons from microstructure fiber”. In: *Optics Express* 12.14 (2004), pp. 3086–3094.
- [18] JG Rarity et al. “Photonic crystal fiber source of correlated photon pairs”. In: *Optics express* 13.2 (2005), pp. 534–544.
- [19] Jingyun Fan, Alan Migdall, and LJ Wang. “Efficient generation of correlated photon pairs in a microstructure fiber”. In: *Optics letters* 30.24 (2005), pp. 3368–3370.
- [20] Offir Cohen et al. “Tailored photon-pair generation in optical fibers”. In: *Physical review letters* 102.12 (2009), p. 123603.
- [21] Xiaoying Li et al. “Optical-fiber source of polarization-entangled photons in the 1550 nm telecom band”. In: *Physical review letters* 94.5 (2005), p. 053601.
- [22] Hiroki Takesue and Kyo Inoue. “1.5- μm band quantum-correlated photon pair generation in dispersion-shifted fiber: suppression of noise photons by cooling fiber”. In: *Optics express* 13.20 (2005), pp. 7832–7839.
- [23] Shellee D Dyer, Burm Baek, and Sae Woo Nam. “High-brightness, low-noise, all-fiber photon pair source”. In: *Optics express* 17.12 (2009), pp. 10290–10297.
- [24] Brian J Smith et al. “Photon pair generation in birefringent optical fibers”. In: *Optics express* 17.26 (2009), pp. 23589–23602.

- [25] Jasleen Lugani et al. “Spectrally pure single photons at telecommunications wavelengths using commercial birefringent optical fiber”. In: *Optics Express* 28.4 (2020), pp. 5147–5163.
- [26] D Cruz-Delgado et al. “Fiber-based photon-pair source capable of hybrid entanglement in frequency and transverse mode, controllably scalable to higher dimensions”. In: *Scientific reports* 6 (2016), p. 27377.
- [27] Karsten Rottwitt, Jacob Gade Koefoed, and Erik Nicolai Christensen. “Photon-pair sources based on intermodal four-wave mixing in few-mode fibers”. In: *Fibers* 6.2 (2018), p. 32.
- [28] Cheng Guo et al. “Generation of telecom-band correlated photon pairs in different spatial modes using few-mode fibers”. In: *Optics Letters* 44.2 (2019), pp. 235–238.
- [29] Hamed Pourbeyram and Arash Mafi. “Photon pair generation with tailored frequency correlations in graded-index multimode fibers”. In: *Optics letters* 43.9 (2018).
- [30] Karsten Rottwitt et al. “Quantum information processing using intermodal four-wave mixing in multi-mode optical fibers”. In: *2019 21st International Conference on Transparent Optical Networks (ICTON)* (2019), pp. 1–3.
- [31] Cagin Ekici and Mehmet Salih Dinleyici. “Graded-index optical fiber transverse-spatial-mode entanglement”. In: *Physical Review A* 102.1 (2020), p. 013702.
- [32] E Scott Goudreau et al. “Theory of four-wave mixing of cylindrical vector beams in optical fibers”. In: *JOSA B* 37.6 (2020), pp. 1670–1682.
- [33] Afshin Shamshooli et al. “Toward Generation of Spatially-Entangled Photon Pairs in a Few-Mode Fiber”. In: *CLEO: Applications and Technology*. Optical Society of America. 2020, JTh2A–27.
- [34] Nicolas K Fontaine et al. “Laguerre-Gaussian mode sorter”. In: *Nature communications* 10.1 (2019), pp. 1–7.
- [35] Mario Krenn et al. “Generation and confirmation of a (100× 100)-dimensional entangled quantum system”. In: *Proceedings of the National Academy of Sciences* 111.17 (2014), pp. 6243–6247.
- [36] Gregorius CG Berkhout et al. “Efficient sorting of orbital angular momentum states of light”. In: *Physical review letters* 105.15 (2010), p. 153601.
- [37] Yves Painchaud et al. “Time-resolved identification of modes and measurement of intermodal dispersion in optical fibers”. In: *Applied optics* 31.12 (1992), pp. 2005–2010.
- [38] Harikumar K Chandrasekharan et al. “Observing mode-dependent wavelength-to-time mapping in few-mode fibers using a single-photon detector array”. In: *APL Photonics* 5.6 (2020), p. 061303.
- [39] NA Kaliteevskiy et al. “Two-mode coupling model in a few mode fiber”. In: *Optics and Spectroscopy* 114.6 (2013), pp. 913–916.
- [40] Ohad Lib, Kfir Sulimany, and Yaron Bromberg. “Reconfigurable synthesizer for quantum information processing of high-dimensional entangled photons”. In: *arXiv preprint arXiv:2108.02258* (2021).
- [41] Nicolas K Fontaine et al. “Hermite-Gaussian mode multiplexer supporting 1035 modes”. In: *2021 Optical Fiber Communications Conference and Exhibition (OFC)*. IEEE. 2021, pp. 1–3.
- [42] Shachar Resisi et al. “Wavefront shaping in multimode fibers by transmission matrix engineering”. In: *APL Photonics* 5.3 (2020), p. 036103.
- [43] Artur K Ekert. “Quantum cryptography based on Bell’s theorem”. In: *Physical review letters* 67.6 (1991), p. 661.
- [44] Xiao-Min Hu et al. “Beating the channel capacity limit for superdense coding with entangled ququarts”. In: *Science advances* 4.7 (2018), eaat9304.
- [45] Yu Guo et al. “Advances in quantum dense coding”. In: *Advanced Quantum Technologies* 2.5-6 (2019), p. 1900011.
- [46] Adán Cabello. “Quantum key distribution in the Holevo limit”. In: *Physical Review Letters* 85.26 (2000), p. 5635.
- [47] Gui-Lu Long and Xiao-Shu Liu. “Theoretically efficient high-capacity quantum-key-distribution scheme”. In: *Physical Review A* 65.3 (2002), p. 032302.
- [48] Fu-Guo Deng, Gui Lu Long, and Xiao-Shu Liu. “Two-step quantum direct communication protocol using the Einstein-Podolsky-Rosen pair block”. In: *Physical Review A* 68.4 (2003), p. 042317.

- [49] Elham Nazemosadat, Hamed Pourbeyram, and Arash Mafi. “Phase matching for spontaneous frequency conversion via four-wave mixing in graded-index multimode optical fibers”. In: *JOSA B* 33.2 (2016), pp. 144–150.
- [50] Logan G Wright et al. “Multimode nonlinear fiber optics: massively parallel numerical solver, tutorial, and outlook”. In: *IEEE Journal of Selected Topics in Quantum Electronics* 24.3 (2017), pp. 1–16.
- [51] Sivan Trajtenberg-Mills et al. “Simulating Correlations of Structured Spontaneously Down-Converted Photon Pairs”. In: *Laser & Photonics Reviews* 14.3 (2020), p. 1900321.